

Development and performance of a micron-resolution neutron imaging detector at CSNS

Xing-Fen Jiang(蒋兴奋), Wen-Qin Yang(杨文钦), Jun-An Geng(耿君安), Sheng-Xiang Wang(王声翔), Xiao-Juan Zhou(周晓娟), Yan-Feng Wang(王艳凤), Jian-Rong Zhou(周健荣), Jie Chen(陈洁), Cheng-Hua Sun(孙承华), Zhi-Jia Sun(孙志嘉), and Yuan-Bo Chen(陈元柏)

Citation: Chin. Phys. B, 2026, 35 (**7**): 076101. DOI: 10.1088/1674-1056/ae5f05
http://cpb.iphy.ac.cn; http://iopscience.iop.org/cpb

What follows is a list of articles you may be interested in

Development of a large-area ^{3}He tube array neutron detector with frequency reduction capability

Yan-Feng Wang(王艳凤), Li-Xin Zeng(曾莉欣), Liang Xiao(肖亮), Sheng Guo(郭胜), Jing-Jing Ma(马静静), Zhen-Hong Tan(谭振宏), Wu Xie(谢武), Wen-Hai Ji(季文海), Ping Miao(缪平), Hai-Yun Teng(滕海云), Pei-Xun Shen(沈培迅), Qing-Lei Xiu(修青磊), Xing-Fen Jiang(蒋兴奋), Hong Xu(许虹), Xiao-Juan Zhou(周晓娟), Meng-Qi Jiang(蒋孟奇), Lin Zhu(朱林), Lei Hu(胡磊), Jia-Jie Li(李嘉杰), Yong-Xiang Qiu(邱勇翔), Jian Zhuang(庄建), Yu-Bin Zhao(赵豫斌), Yuan-Bo Chen(陈元柏), Jian-Rong Zhou(周健荣), and Zhi-Jia Sun(孙志嘉)
Chin. Phys. B, 2025, 34 (**11**): 116102. DOI: 10.1088/1674-1056/adfefd

A large-area scintillation neutron detector based on WLSF and SiPM readout

Xiao-Hu Wang(王小胡), Yang-Tu Lu(卢扬图), Bin Tang(唐彬), Xiu-Ku Wang(王修库), Shao-Jia Chen(陈少佳), Ze-Ren Li(李泽仁), and Zhi-Jia Sun(孙志嘉)
Chin. Phys. B, 2025, 34 (**6**): 066106. DOI: 10.1088/1674-1056/adcb1c

Performance optimization of the neutron-sensitive image intensifier used in neutron imaging

Jinhao Tan(谭金昊), Yushou Song(宋玉收), Jianrong Zhou(周健荣), Wenqin Yang(杨文钦), Xingfen Jiang(蒋兴奋), Jie Liu(刘杰), Chaoyue Zhang(张超月), Xiaojuan Zhou(周晓娟), Yuanguang Xia(夏远光), Shulin Liu(刘术林), Baojun Yan(闫保军), Hui Liu(刘辉), Songlin Wang(王松林), Yubin Zhao(赵豫斌), Jian Zhuang(庄建), Zhijia Sun(孙志嘉), and Yuanbo Chen(陈元柏)
Chin. Phys. B, 2024, 33 (**8**): 086102. DOI: 10.1088/1674-1056/ad47ad

First neutron Bragg-edge imaging experimental results at CSNS

Jie Chen(陈洁), Zhijian Tan(谭志坚), Weiqiang Liu(刘玮强), Sihao Deng(邓司浩), Shengxiang Wang(王声翔), Liyi Wang(王立毅), Haibiao Zheng(郑海彪), Huaile Lu(卢怀乐), Feiran Shen(沈斐然), Jiazheng Hao(郝嘉政), Xiaojuan Zhou(周晓娟), Jianrong Zhou(周健荣), Zhijia Sun(孙志嘉), Lunhua He(何伦华), and Tianjiao Liang(梁天骄)
Chin. Phys. B, 2021, 30 (**9**): 096106. DOI: 10.1088/1674-1056/ac0da7

INSTRUMENTATION AND MEASUREMENT

Development and performance of a micron-resolution neutron imaging detector at CSNS

Xing-Fen Jiang(蒋兴奋)[1,2], Wen-Qin Yang(杨文钦)[1,2], Jun-An Geng(耿君安)[2,4], Sheng-Xiang Wang(王声翔)[1,2], Xiao-Juan Zhou(周晓娟)[1,2], Yan-Feng Wang(王艳凤)[1,2], Jian-Rong Zhou(周健荣)[1,2,3,†], Jie Chen(陈洁)[1,2,3,‡], Cheng-Hua Sun(孙承华)[5,§], Zhi-Jia Sun(孙志嘉)[1,2,3], and Yuan-Bo Chen(陈元柏)[1,2,3]

[1] *Institute of High Energy Physics, Chinese Academy of Sciences, Beijing* 100049, *China*
[2] *Spallation Neutron Source Science Center, Dongguan* 523803, *China*
[3] *University of Chinese Academy of Sciences, Beijing* 100049, *China*
[4] *School of Physics, State Key Laboratory of Optoelectronic Materials and Technologies, Sun Yat-sen University, Guangzhou* 510275, *China*
[5] *Key Laboratory of Photochemical Conversion and Optoelectronic Materials, Technical Institute of Physics and Chemistry, Chinese Academy of Sciences, Beijing* 100190, *China*

(Received 26 February 2026; revised manuscript received 10 April 2026; accepted manuscript online 14 April 2026)

Neutron imaging is a powerful non-destructive testing technique, yet its spatial resolution remains considerably inferior to that of x-ray imaging. Bridging this resolution gap to the micron level represents a major challenge in the field. This study reports the development and performance of a micron-resolution neutron imaging detector at the China Spallation Neutron Source (CSNS). The detector consisted of a custom-fabricated, ultra-thin (5 μm) scintillator based on isotopically enriched gadolinium oxysulfide ($^{157}Gd_2O_2S$:Tb), coupled with a high-magnification optical lens and a scientific charge-coupled device (CCD) camera. At the Energy-Resolved Neutron Imaging Instrument (ERNI), the detector achieved a spatial resolution of 6.6 μm. The detector represents a significant leap in imaging capability at CSNS, enabling advanced non-destructive investigations at the microscale.

Keywords: high-resolution neutron imaging, isotopically enriched gadolinium oxysulfide, ultra-thin scintillator, neutron detector

PACS: 61.05.Tv, 28.20.Pr, 29.40.Mc

DOI: 10.1088/1674-1056/ae5f05 **CSTR:** 32038.14.CPB.ae5f05

1. Introduction

Neutron imaging has been widely employed as a powerful non-destructive technique across a diverse spectrum of research domains, including materials science, archaeology, industrial non-destructive testing, renewable energy, and biomedical science.[1] Owing to their neutral charge and magnetic moment, neutrons interact with atomic nuclei, enabling them to penetrate thick metallic layers while maintaining high sensitivity to light elements such as hydrogen, lithium, and boron. This complementary nature to x-ray imaging, which is more sensitive to electron density, renders neutron imaging a unique tool for probing material internal structures and dynamic processes. However, a significant resolution gap persists between these two modalities. While laboratory-based x-ray micro-computed tomography systems routinely achieve spatial resolutions below 10 μm, and even sub-micron resolutions are attainable at high-brightness x-ray sources, the spatial resolution offered at most neutron facilities typically remains at the tens of microns level for regular user experiments. Therefore, the capability to achieve sub-10 μm resolution in neutron imaging is a critical requirement within the scientific community, crucial for addressing pivotal challenges such as visualizing water distribution within operating fuel cells,[2,3] tracking lithium migration and dendrite formation in batteries,[4,5] and characterizing hydrogen diffusion and precipitation in nuclear fuel cladding.[6]

Substantial efforts have been dedicated to improving the spatial resolution of neutron imaging.[7,8] The mainstream approach, based on scintillator-coupled optical imaging systems, has seen progressive advancements. Notable milestones include the demonstration of 7.6 μm resolution using a 4-μm thick Gd_2O_2S:Tb (GOS) scintillator within the Paul Scherrer Institute (PSI) "Neutron Microscope" project,[9] which was later improved to 4.2 μm by employing isotopically enriched $^{157}Gd_2O_2S$:Tb (^{157}GOS) scintillators at the Institute Laue-Langevin (ILL).[10] A GOS:Tb scintillator additionally doped with F was used at the Institute of Nuclear Physics and Chemistry to enhance the fluorescence intensity, achieving a spatial resolution of 12 μm.[11] The use of a high-transparency single-

†Corresponding author. E-mail: zhoujr@ihep.ac.cn
‡Corresponding author. E-mail: chenjie@ihep.ac.cn
§Corresponding author. E-mail: sunchenghua@mail.ipc.ac.cn

© 2026 Chinese Physical Society and IOP Publishing Ltd. All rights, including for text and data mining, AI training, and similar technologies, are reserved.

crystal $Gd_3Ga_5O_{12}$:Eu (GGG:Eu) scintillator integrated with an infinity-corrected optical system enabled an isotropic spatial resolution below 4 μm.[7]

Beyond the conventional optical magnification route, other innovative methods have been explored. A tilted detector setup has been demonstrated to provide substantial resolution improvement along the tilting axis, but the reported resolution was only 20 μm.[12] Another promising development involves axisymmetric neutron focusing mirrors, known as Wolter optics, which aim to achieve micrometer or even sub-micrometer resolution through direct magnification in the neutron beam path. However, the current resolution of this technique remains on the scale of several tens of micrometers.[13,14] The event centroid method represents another approach, aiming to surpass the intrinsic resolution of detectors by precisely locating individual neutron interaction events. Neutron-sensitive microchannel plate (MCP) detectors combined with high-speed readout chips like Timepix enable this mode, though the resolution is ultimately limited by the MCP pore size (typically 11–15 μm).[15] Similarly, incorporating an image intensifier into a scintillator-sCMOS system allows for single-event reconstruction, achieving a remarkable 2 μm resolution at the National Institute of Standards and Technology (NIST), albeit requiring the acquisition of tens of thousands of frames per radiography, which poses challenges for practical application.[16] Despite these promising developments, the scintillator-based imaging approach coupled with high-magnification optics remains the most mature and widely applicable technique for achieving micron-level resolution in operational settings.

At the China Spallation Neutron Source (CSNS), the development of neutron imaging technologies has progressed since its construction phase. Previous achievements include a spatial resolution below 18 μm (line width) using a 10 μm thick GOS:Tb scintillator and a scientific charge-coupled device (CCD) camera.[17] Furthermore, energy-resolved neutron imaging detectors based on time-stamping cameras have been developed, achieving a resolution of 20 μm with event reconstruction techniques.[18,19] Building upon this legacy and the global pursuit of higher resolution, this work presents the development and performance of a high-resolution thermal neutron imaging detector at CSNS. The detector utilized a custom-fabricated, 5 μm thick ultra-thin scintillator screen based on isotopically enriched ^{157}GOS. Coupled with a precision optical system and optimized detector design, it was characterized at the Energy-Resolved Neutron Imaging Instrument (ERNI).[20] The detector achieved a spatial resolution of 6.6 μm, marking a significant step forward in micron-level neutron imaging capability at CSNS and providing a powerful tool for non-destructive investigation at the micron scale.

2. Scintillator fabrication

2.1. Scintillator simulation

The properties of a 5 μm thick ^{157}GOS (with 88% abundance of ^{157}Gd) scintillator were investigated using the Monte Carlo simulation method based on the Geant4 toolkit. Internal conversion electrons were found to play a dominant role in determining both luminescence efficiency and spatial resolution.

As shown in Fig. 1(a), the energy distribution of internal conversion electrons from gadolinium exhibits major components below 85 keV, resulting in short electron ranges and consequently limited light yield. The simulation reveals that photon accumulation at the scintillator surface forms a characteristic light spot (Fig. 1(b)). By fitting the x-direction projection of this light distribution (Fig. 1(c)), the full width at half maximum (FWHM) was determined to be approximately 6 μm, providing a high intrinsic spatial resolution. To more intuitively demonstrate the spatial resolution characteristics, a star-pattern imaging simulation was performed. As illustrated in Fig. 1(d), the inner features of the star pattern remain visually distinguishable, corresponding to a spatial resolution of 4 μm. Furthermore, based on neutron absorption calculations, the neutron capture efficiency was determined to be 92%, highlighting the superior detection efficiency of the ^{157}GOS scintillator.

2.2. Preparation of the ultra-thin scintillator

The ^{157}GOS scintillator material was synthesized via a high-temperature solid-state reaction, following the procedure illustrated in Fig. 2(a). Stoichiometric quantities of $^{157}Gd_2O_3$, S, Tb_4O_7, and Na_2CO_3 were precisely weighed and homogeneously mixed by grinding in an agate mortar for 15 minutes. The resulting uniform mixture was transferred to a crucible and heated in a tube furnace at 900 °C for 4 hours under a controlled reducing atmosphere (8 vol% H_2/92 vol% Ar). After heat treatment and cooling to room temperature, the product was washed to remove soluble byproducts and dried at 80 °C, yielding the final ^{157}GOS:Tb phosphor powder.

The synthesized phosphor powder was initially characterized by scanning electron microscopy (SEM) to evaluate particle size and morphology. As shown in Fig. 2(b), the particles exhibited a size distribution ranging from several hundred nanometers to approximately 2 micrometers, demonstrating uniformity that is favorable for fabricating homogeneous scintillation screens. X-ray diffraction (XRD) analysis confirmed the formation of the GOS phase for both isotopically enriched ^{157}Gd and natural Gd samples, with diffraction patterns matching well with the standard reference (PDF#26-1422, Fig. 2(c)). Photoluminescence (PL) spectra of the GOS:Tb material under 285 nm excitation (Fig. 2(d)) revealed a series of sharp emission bands between 300–800 nm, with the most intense peak at 544 nm corresponding to the $^5D_4 \rightarrow {}^7F_5$ electronic

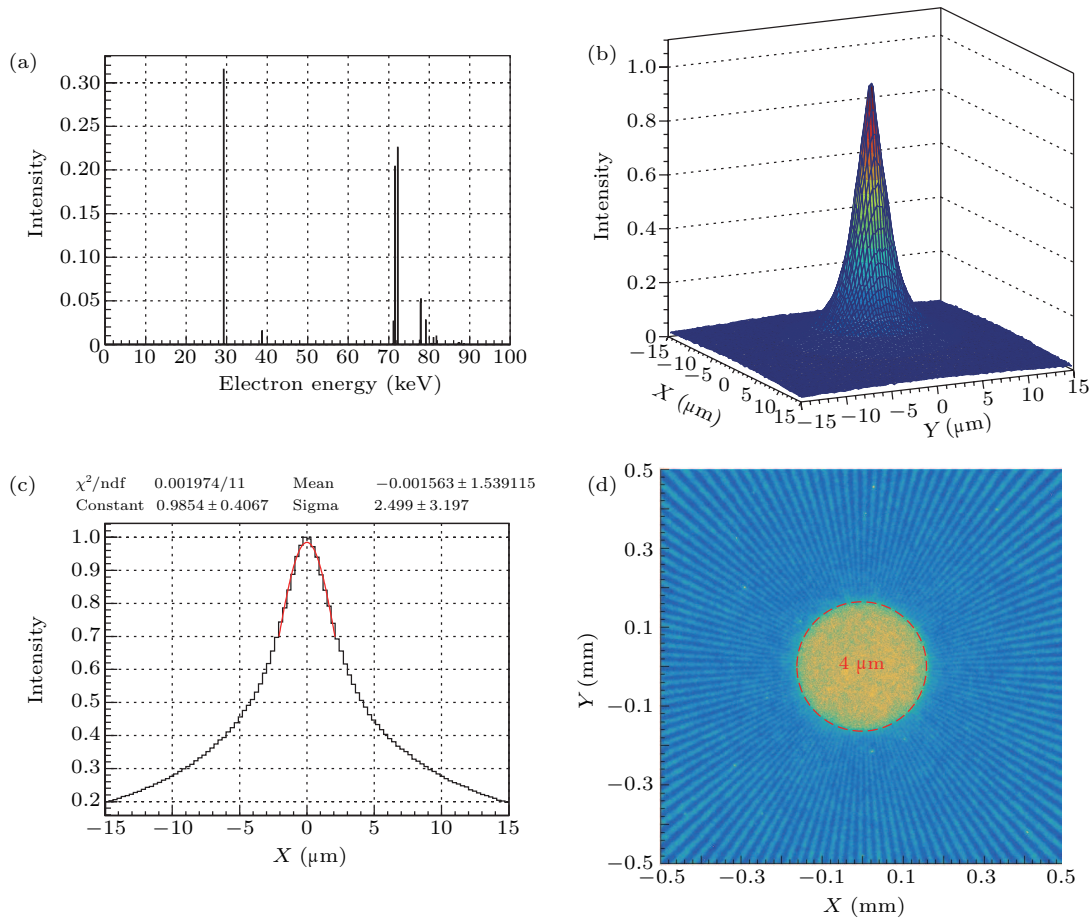


Fig. 1. Simulation results of GOS scintillator: (a) the distribution of the energy of internal conversion electrons, (b) the light spot, (c) the *x*-direction projection, and (d) the imaging simulation of a star-pattern test target.

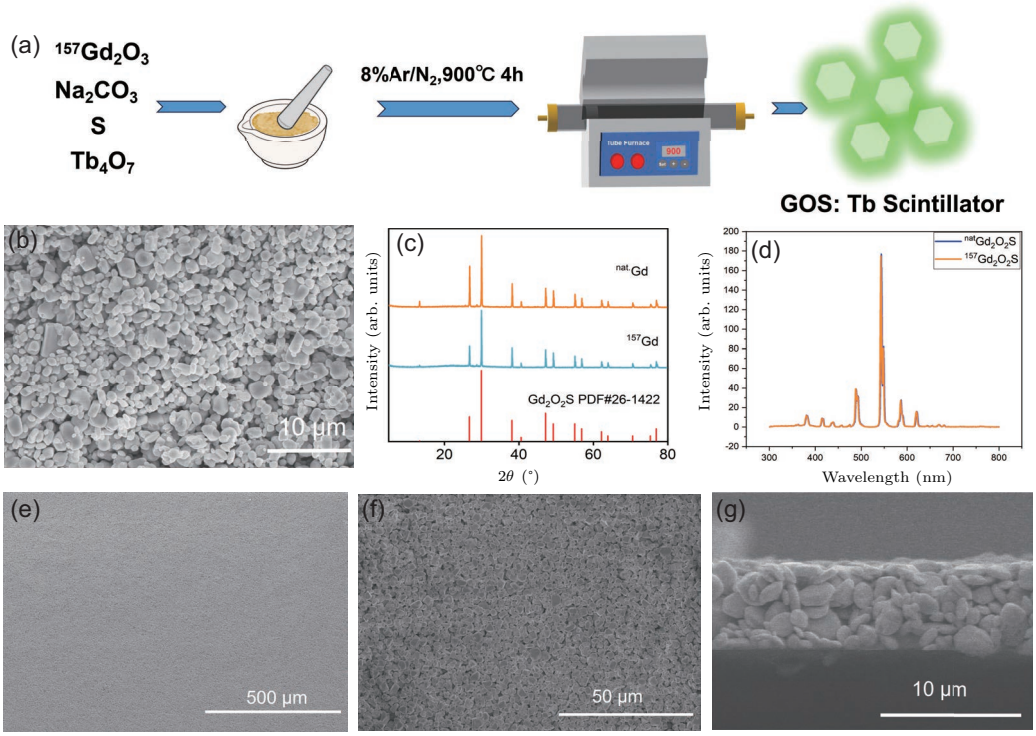


Fig. 2. (a) A schematic diagram of the high-temperature synthesis procedure of the fluorescent material; (b) SEM image of the as-synthesized ^{157}GOS particles, showing a size distribution from hundreds of nanometers to several micrometers; (c) XRD patterns of fluorescent materials prepared from natural Gd (^{nat}Gd) and isotopically enriched ^{157}Gd, both matching the standard GOS phase (PDF#26–1422); (d) fluorescence spectrum of the fluorescent material; (e) and (f) surface morphology of the ultra-thin scintillator under low and high magnification SEM; and (g) cross-sectional SEM view of the scintillator.

transition of Tb^{3+}. The fluorescence intensities were essentially identical for both Gd isotopes, indicating that isotopic enrichment did not compromise the luminescent properties.

To fabricate the ultra-thin scintillator, the phosphor powder was uniformly dispersed in a film-forming polymer binder. The slurry was coated onto an aluminum substrate using a sequential drop-casting and spin-coating approach. During drop-casting, density-driven settling of ^{157}GOS particles facilitated the formation of a dense fluorescent layer. The subsequent spin-coating process effectively removed excess binder and solvent, reducing the polymer content and significantly enhancing the packing density. SEM analysis of the fabricated scintillator demonstrated a uniform and densely packed surface morphology at both low and high magnifications (Figs. 2(e)–2(g)), with no significant agglomeration or voids observed. Cross-sectional imaging (Fig. 2(g)) confirmed a consistent thickness of approximately 5 μm, a key parameter for ensuring high spatial resolution and grayscale homogeneity in neutron imaging applications.

2.3. Light output measurement

The light output of the 5 μm thick scintillator was measured on the BL-20 beamline at CSNS. The experimental setup is illustrated in Fig. 3. Due to the relatively weak luminescence of the scintillator, the measurement of light output is highly susceptible to gamma-ray interference. To mitigate this effect, gamma-ray suppression was achieved by combining physical shielding with pulse time-window selection.

A monochromator was positioned at a 45° tilt angle along the neutron beam path to provide a monochromatic neutron beam and eliminate most of the gamma-ray background from the source. The detection system consisted of a photomultiplier tube (PMT, Hamamatsu XP2020) housed within a light-tight chamber, with the PMT optically coupled in direct contact with the scintillator screen. The entire assembly was surrounded by lead bricks to attenuate environmental stray gamma-rays. For data acquisition, a high-precision digitizer (CAEN DT5730) located outside the shielding chamber recorded the charge spectrum produced by the scintillator-PMT combination. Crucially, by leveraging the intrinsic time structure of the pulsed spallation neutron source, the gamma-induced background was further suppressed by synchronizing the data acquisition trigger exclusively with the time window corresponding to the arrival of monochromatic neutrons.

The resulting charge spectrum is presented in Fig. 4, showing a distinct peak at 60.61 ADC channels, which corresponds to a collected charge of 19.15 pC. Taking into account the PMT operating voltage of 2000 V (yielding a gain of 7.95×10^6) and its quantum efficiency of approximately 6% at the scintillator's characteristic emission wavelength of 544 nm, the light output of the scintillator was determined to be 250 ± 0.7 photons per neutron (ph/n), where 0.7 ph/n is the statistical error.

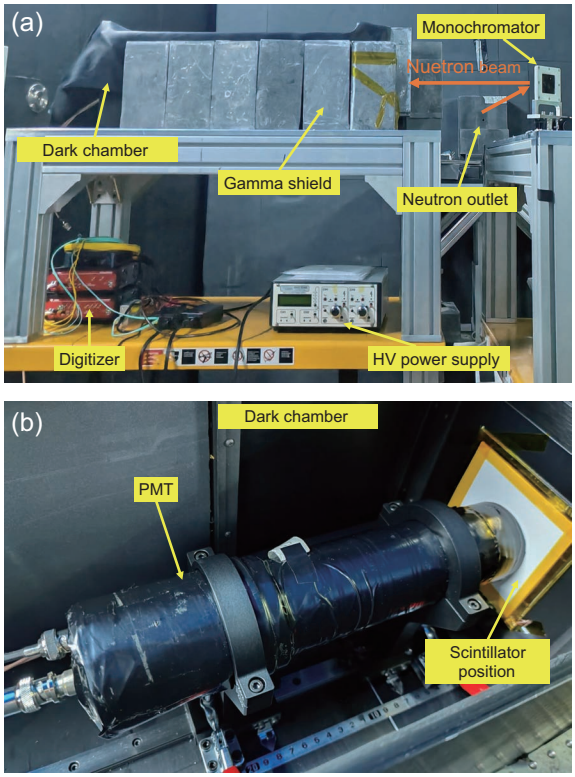


Fig. 3. Experimental setup for light-output measurement: (a) experimental system at BL-20; (b) the light-tight chamber.

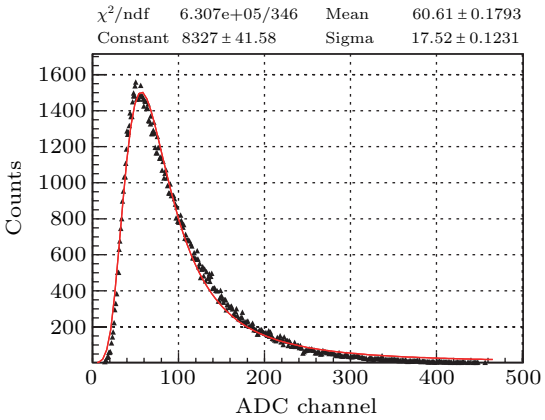


Fig. 4. Measured charge spectrum of single-neutron events in the scintillator.

3. Detector design and assembly

The structural design of the high-resolution neutron imaging detector is schematically illustrated in Fig. 5. The system was optimized to achieve micron-level spatial resolution. A compact scintillator holder assembly incorporating a miniature mirror was designed to minimize the scintillator-to-mirror distance, ensuring compatibility with the short working distance required for high-magnification imaging lenses. The complete detection assembly was housed within a light-tight enclosure equipped with bellows to eliminate ambient light interference. Furthermore, the detector was shielded with AlB alloy plates

to attenuate scattered neutrons, thereby reducing the imaging background and minimizing potential radiation damage to the camera. The camera, coupled with a high-magnification lens, was mounted on a motorized translation stage. By finely adjusting the stage via an automatic focusing system, a clearly focused state can be efficiently achieved. To enable rapid and precise focusing, an integrated light-emitting diode (LED) projector was installed inside the chamber to project a high-contrast grid pattern onto the scintillator screen. This method significantly reduced focusing time by utilizing the intense LED illumination source, as opposed to relying on the inherently weak scintillation signal, thereby optimizing the utilization of valuable neutron beam time.

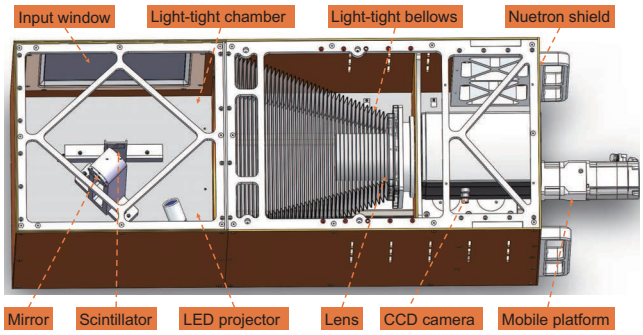


Fig. 5. The schematic structure of the detector.

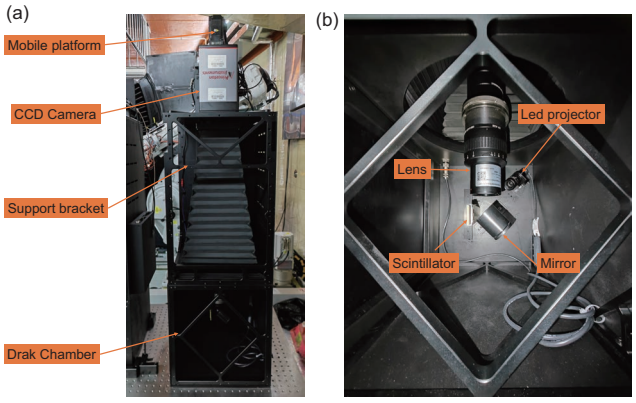


Fig. 6. The detector assembly: (a) whole view, (b) internal perspective of the light-tight chamber.

As demonstrated in Fig. 6, the detector system was assembled on an optical platform at ERNI. The core imaging component is a scientific-grade CCD camera, featuring a pixel size of 15 μm × 15 μm, an array of 2048 × 2048 pixels, and thermoelectric cooling to −80 °C for low-noise operation. An isotopically enriched ^{157}GOS scintillator with a thickness of 5 μm and an area of 30 mm × 30 mm was used. A high-performance lens (XENON-DIAMOND 2.2/117, Schneider) was selected to provide the necessary optical magnification. During imaging characterization, the lens was configured at 4.8× magnification, resulting in an effective pixel size of approximately 3.1 μm × 3.1 μm at the scintillator plane and a field of view of 6.4 mm × 6.4 mm. Following assembly, the entire system was adjusted to a well-focused state, establishing a solid foundation for high-resolution neutron imaging.

4. Experiment and results

4.1. Experimental environment at ERNI

The ERNI facility is the first neutron imaging instrument at CSNS, specifically designed as a multi-scale, multi-dimensional, and multi-modality characterization platform. The schematic diagram of the experiment layout at ERNI is presented in Fig. 7. The instrument utilizes pulsed neutrons moderated by a coupled hydrogen moderator (CHM) and enhanced by two super-mirror neutron guides to provide a high neutron flux and a large, uniform imaging field. A chopper system, including a T0 chopper, two single-disk choppers, and one double-disk chopper, is equipped to remove fast neutrons and gamma radiation and to precisely select specific neutron wavelength bands. With a pinhole selector installed at 24.78 m from the CHM and two sample stages positioned at 30 mm (stage 1) and 35 m (stage 2) respectively, a wide range of collimation ratios can be achieved.[20]

The imaging resolution is primarily influenced by the neutron flux, the collimation ratio, and the intrinsic spatial resolution of the detector. Considering the compatibility of these factors, the imaging experiment was conducted at sample stage 2. A pinhole with a diameter of 10 mm was selected, yielding a collimation ratio better than 1000, and the neutron wavelength was set to 2–6.1 Å by neutron choppers. The detector was securely held by a hexapod robotic arm, offering sub-micrometer precision in six degrees of freedom, and was meticulously aligned to the center of the neutron beam (Fig. 8).

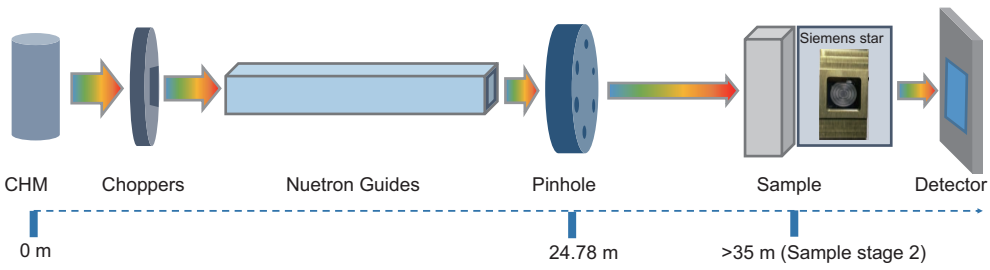


Fig. 7. The schematic diagram of the experiment layout at ERNI.

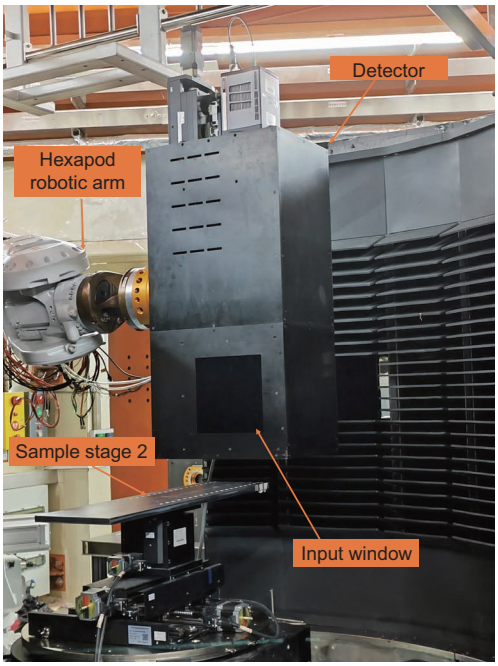


Fig. 8. The neutron imaging testing of the detector at ERNI.

4.2. Imaging results

The spatial resolution performance of the developed neutron imaging detector was quantitatively evaluated using a gadolinium Siemens-star test target with 128 line pairs, with a spatial resolution range spanning from 4 μm to 250 μm. The Siemens star pattern offers distinct advantages for resolution assessment, enabling continuous spatial frequency sampling across its radial structure. Visual inspection confirmed that the smallest distinguishable pattern corresponds to a spatial resolution of 6.6 μm (Fig. 9).

To provide an objective and quantitative assessment of the detector's performance, the modulation transfer function (MTF) was calculated from the imaging data. The resulting MTF curve, plotted in Fig. 10, exhibited the expected monotonic decrease with increasing spatial frequency. In imaging system characterization, the resolution limit is conventionally defined as the spatial frequency at which the MTF reaches a specified threshold value. Our analysis indicated that a line pair density of 73.6 lp/mm was achieved at the 5% MTF threshold, corresponding to a spatial resolution of 6.8 μm. This result is in excellent agreement with the visual resolution estimate of 6.6 μm derived from the Siemens-star image, thereby providing robust and consistent validation of the detector's micron-level resolution capability.

The successful realization of micron-level spatial resolution demonstrates that the developed detector system, integrating the ultra-thin isotopically enriched scintillator with the precision optical configuration, effectively addresses a critical performance gap in neutron imaging technology. This advancement enables high-resolution non-destructive investigations at the micron scale, opening new possibilities for materials characterization and defect analysis in various scientific and industrial applications at CSNS.

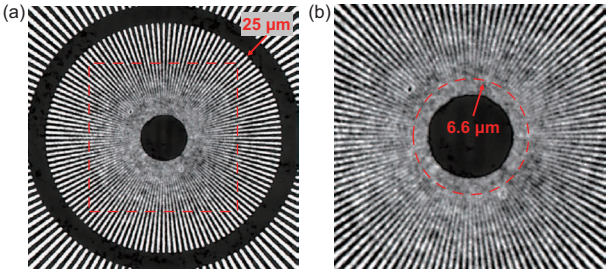


Fig. 9. (a) Neutron imaging results of a Siemens star test target; (b) magnified view of the region marked by the red box.

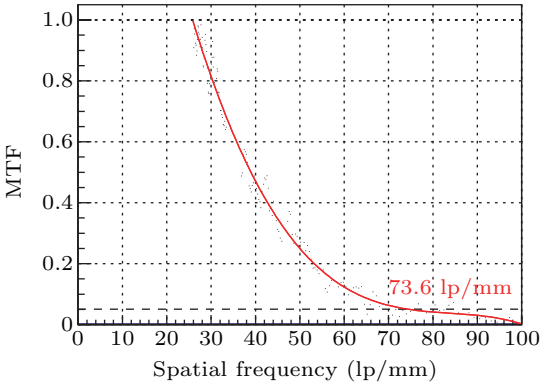


Fig. 10. The MTF curve of the Siemens Star image.

5. Conclusion

A high-resolution neutron imaging detector capable of micron-level spatial resolution has been successfully developed and commissioned at CSNS. A 5 μm thick, isotopically enriched ^{157}GOS scintillator was fabricated, which provides high intrinsic spatial resolution while maintaining excellent neutron absorption efficiency. Under irradiation on the BL-20 beamline at CSNS, the scintillator demonstrated a light output of 250 ± 0.7 ph/n. The scintillator was efficiently coupled with a precision optical system featuring $4.8\times$ magnification and a scientific-grade CCD camera to form the imaging detector. The integrated detector system was characterized under high collimation ratio (> 1000) conditions at ERNI. The spatial resolution was assessed using a gadolinium-coated Siemens star. Line pairs corresponding to a spatial resolution of 6.6 μm were distinguished, while modulation transfer function (MTF) analysis yielded a resolution of 6.8 μm at the 5% MTF threshold.

The successful development and demonstration of this detector provides the scientific community with a powerful and reliable tool for non-destructive micro-scale investigations at CSNS. Future work will focus on further optimizing the scintillator composition and fabrication process to push the resolution towards the sub-5 μm regime and applying this tool to address specific scientific problems requiring micron-scale insight into material structure and dynamics.

Acknowledgments

Project supported by the Science Challenge Project (Grant No. TZ2025014), the National Key Research and Development Program of China (Grant No. 2025YFF0520801), the Space Application System of China Manned Space Program (Grant No. CMSS-2024-4-A-002), the National Natural Science Foundation of China (Grant Nos. 12305348, 12527806, 12227810, and 52472206), the Guangdong Basic and Applied Basic Research Foundation (Grant Nos. 2025A1515011320 and 2024B1515120006), the Guangdong Provincial Key Laboratory of Advanced Particle Detection Technology (Grant No. 2024B1212010005), the CAS Project for Young Scientists in Basic Research (Grant No. YSBR-024), the Guangdong S&T Programme (Grant No. 2023A1111120019), the Beijing Nova Program (Grant No. 202504841009), and the Open Fund of the China Spallation Neutron Source Songshan Lake Science City (Grant No. KFKT2023A05).

We also thank the staff members of the Energy-resolved Neutron Imaging Instrument (https://csns.cn/31113.02.CSNS.ERNI) at the China Spallation Neutron Source (CSNS) (https://csns.cn/31113.02.CSNS), for providing technical support and assistance.

References

[1] Kardjilov N, Manke I, Woracek R, Hilger A and Banhart J 2018 *Mater. Today* **21** 652
[2] Manke I, Hartnig C, Kardjilov N, Messerschmidt M, Hilger A, Strobl M, Lehnert W and Banhart J 2008 *Appl. Phys. Lett.* **92** 244101
[3] Satija R, Jacobson D L, Arif M and Werner S A 2004 *J. Power Sources* **129** 238
[4] Song B H, Dhiman I, Carothers J C, Veith G M, Liu J, Bilheux H Z and Huq A 2019 *ACS Energy Lett.* **4** 2402
[5] Golozar M, Hovington P, Paolella A, Bessette S, Lagace M, Bouchard P, Demers H, Gauvin R and Zaghib K 2018 *Nano Lett.* **18** 7583
[6] Gong W J, Trtik P, Ma F Q, Jia Y X, Li J S and Bertsch J 2022 *J. Nucl. Mater.* **570** 153971
[7] Tengattini A, Kardjilov N, Helfen L, Douissard P A, Lenoir N, Markotter H, Hilger A, Arlt T, Paulisch M, Turek T and Manke I 2022 *Opt. Express* **30** 14461
[8] Trtik P and Lehmann E H 2016 *VI European Conference on Neutron Scattering*, August 30–September 4, 2015, Zaragoza, Spain, p. 012004
[9] Trtik P, Hovind J, Gruenzweig C, Bollhalder A, Thominet V, David C, Kaestner A and Lehmann E H 2015 *Phys. Procedia* **69** 169
[10] Trtik P, Meyer M, Wehmann T, Tengattini A, Atkins D, Lehmann E H and Strobl M 2020 *The 11th World Conference on Neutron Radiography*, September 2–7, 2018, Sydney, Australia, pp. 23
[11] Tang B, Yin W, Wang Q B, Chen L, Huo H Y, Wu Y, Yang H C, Sun C H and Zhou S Y 2023 *Molecules* **28** 1815
[12] Boillat P, Kramer D, Seyfang B C, Frei G, Lehmann E H, Scherer G G, Wokaun A, Ichikawa Y, Tasaki Y and Shinohara K 2008 *Electrochim. Commun.* **10** 546
[13] Liu D, Hussey D, Gubarev M V, Ramsey B D, Jacobson D, Arif M, Moncton D E and Khaykovich B 2013 *Appl. Phys. Lett.* **102** 183505
[14] Abir M, Hussey D S and Khaykovich B 2020 *J. Imaging* **6** 100
[15] Tremsin A S, Morgano M, Panzner T, Lehmann E H, Filgers U, Vallerga J V, McPhate J B, Siegmund O H W and Feller W B 2015 *Nucl. Instrum. Methods Phys. Res. A* **784** 486
[16] Hussey D S, LaManna J M, Baltic E and Jacobson D L 2017 *Nucl. Instrum. Methods Phys. Res. A* **866** 9
[17] Jiang X F, Xiu Q L, Zhou J R, Yang J Q, Tan J H, Yang W Q, Zhang L J, Xia Y G, Zhou X J, Zhou J J, Zhu L, Teng H Y, Yang G A, Song Y S, Sun Z J and Chen Y B 2021 *Nucl. Eng. Technol.* **53** 1942
[18] Yang J Q, Zhou J R, Jiang X F, Tan J H, Zhang L J, Zhou J J, Zhou X J, Yang W Q, Xia Y G, Chen J, Sun X L, Zhang Q H, Li J, Sun Z J and Chen Y B 2021 *Nucl. Instrum. Methods Phys. Res. A* **1000** 165222
[19] Yang W Q, Zhou J R, Yang J Q, Jiang X F, Tan J H, Zhu L, Zhou X J, Xia Y G, Yu L, Wang X K, Teng H Y, Li J J, Qiu Y X, Shen P X, Wang S L, Wei Y D, Song Y S, Zhuang J, Zhao Y B, Zhang J R, Sun Z J and Chen Y B 2024 *Nucl. Eng. Technol.* **56** 2799
[20] Chen J, Yu C J, Zeng Z R, Zheng H B, Wang S X, Tan Z J, Yang L F, Wang L Y and Zhang X K 2024 *Nucl. Instrum. Methods Phys. Res. A* **1064** 169460